13th Australasian Fluid Mechanics Conference
Monash University, Melbourne, Australia
13-18 December 1998

MODELING ROD-CLIMBING OF VISCOELASTIC FLUIDS WITH ORTHOGONAL TRAJECTORY GRIDS

Xiao-Lin LUO

CSIRO Mathematical and Information Sciences
North Ryde, New South Wales, AUSTRALIA

ABSTRACT

A finite element simulation of the Weissenberg effect, *i.e.* the rod climbing of viscoelastic fluids, is presented. The flow features axisymmetric swirling, free surface, gravity, surface tention, centrifugal force and all six viscoelastic stresses. An operator splitting algorithm is employed to solve the non-linear system of equations governing the upper-convected Maxwell or the Phan-Thien–Tanner fluid. An orthogonal trajectory scheme applicable to unstructured as well as structured grids is adopted to construct the mesh after each free surface updating. Comparison between numerical and experimental results shows good agreement.

INTRODUCTION

It is well known that fluids with complex structure, such as macromolecular solutions and melts, behave in unexpected ways which can not be described by Newton's viscous law. The Weissenberg effect (Weissenberg 1947) is one of the most interesting phenomena exhibited by non-Newtonian fluids: certain viscoelastic fluids in a cylindrical vessel will climb up a rotating rod against centrifugal force and gravity. The rod-climbing is one of the many second-order effects associated with the inequality of normal stresses in shear flow (Brid *et al* 1987, Tanner 1985). It was suggested (Barnes *el.* 1989) that the normal stress acts like a hoop around the rod and forces the fluid inwards against the centrifugal force and upwards against the gravitational force. Numerical, analytical and experimental studies of this phenomena will improve the understanding of the rheological properties of non-Newtonian fluids and enable us to better predict many natural and industrial non-Newtonian flows.

The present work explores new ways to overcome the difficulties encountered in rod-climbing simulation. An elaborate mesh updating scheme is developed to minimize mesh distortion by making use of orthogonal or nearly orthogonal trajectory functions. Both the structured quadrilateral mesh and the unstructured triangular mesh will be used in the simulation to check the mesh-independence of the solutions.

GOVERNING EQUATIONS

The motion of an incompressible viscoelastic fluid is governed by the following equations

$$\rho[\frac{\partial \mathbf{u}}{\partial t} + (\mathbf{u}\cdot\nabla)\mathbf{u}] - \eta\Delta\mathbf{u} + \nabla p = \rho\mathbf{g} + \nabla\cdot\tau \quad (1)$$

$$\nabla\cdot\mathbf{u} = 0 \quad (2)$$

where η is the sum of solvent and molecular viscosities, $\mathbf{u}$ is velocity, p is pressure, $\mathbf{g}$ is gravity and τ is the extra viscoelastic stress tensor defined by,

$$\tau \equiv \sigma + p\mathbf{I} - 2\eta\mathbf{d} \quad (3)$$

where σ is the total stress tensor. For UCM fluid the extra viscoelastic stress satisfies the following constitutive equation

$$\lambda(\frac{\partial \tau}{\partial t} + \mathbf{u}\cdot\nabla\tau - \mathbf{L}\tau - \tau\mathbf{L}^T) + \tau = -2\lambda\eta_m(\frac{\partial \mathbf{d}}{\partial t} + \mathbf{u}\cdot\nabla\mathbf{d} - \mathbf{L}\mathbf{d} - \mathbf{d}\mathbf{L}^T) \quad (4)$$

where λ is the relaxation time, η_m is the molecular viscosity, $\mathbf{L} = \nabla\mathbf{u}^T$ is the velocity gradient tensor, $\mathbf{d} = (\mathbf{L} + \mathbf{L}^T)/2$ is the rate of deformation tensor. The Phan-Thein-Tanner (PTT) model can also be expressed in terms of τ

$$\lambda[\frac{\partial \tau}{\partial t} + \mathbf{u}\cdot\nabla\tau - (\mathbf{L} - \xi\mathbf{d})\tau - \tau(\mathbf{L} - \xi\mathbf{d})^T] + [1 + (\epsilon\lambda/\eta_m)tr\tau]\tau + (2\epsilon\lambda tr\tau)\mathbf{d} = -2\lambda\eta_m[\frac{\partial \mathbf{d}}{\partial t} + \mathbf{u}\cdot\nabla\mathbf{d} - (\mathbf{L} - \xi\mathbf{d})\mathbf{d} - \mathbf{d}(\mathbf{L} - \xi\mathbf{d})^T] \quad (5)$$

where $tr\tau$ is the trace of τ, ξ is a material parameter controlling the ratio of second to first normal stress difference, and ϵ is related to elongational viscosity. In the case of axisymmetric swirling flow, we have altogether ten unknown variables: three velocity components u_r, u_z and u_θ, pressure p and six extra viscoelastic stresses τ_{rr}, τ_{rz},τ_{zz},$\tau_{\theta\theta}$, $\tau_{r\theta}$ and $\tau_{z\theta}$.

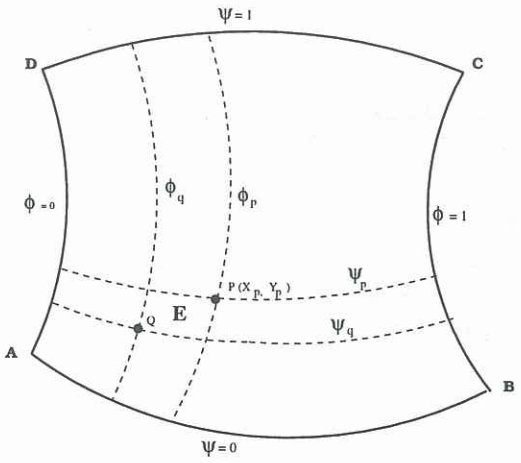

Figure 1: An illustration of orthogonal trajectory mesh.

NUMERICAL SCHEME

An operator splitting algorithm (Dean *et al.* 1988, Luo 1996) is employed to solve the non-linear system of equations governing the upper-convected Maxwell or the Phan-Thien–Tanner fluid. Our free surface scheme mainly consists of three steps:

I) track explicitly the moving boundary and generate an intermediate mesh in the new domain;

II) find a pair of orthogonal or nearly orthogonal trajectory functions in the new domain using the intermediate mesh;

III) adjust the mesh according to the orthogonal trajectories to minimize mesh distortion while maintaining the free surface shape.

We will adopt Fastflo's existing free surface module (Mooney & de Hoog, 1995) to track the moving boundary, in which we solve for a normal displacement function $h(s)$ on the free surface satisfying the differential equation

$$\frac{h}{\Delta t}+\mathbf{u}^{n+1}\cdot\mathbf{t}\,\frac{\delta h}{\delta s}-\alpha\frac{\delta^2 h}{\delta s^2}=\mathbf{u}^{n+1}\cdot\mathbf{n}\ \text{ on }\ \delta\Omega_f \quad (6)$$

With normal displacement of free surface known, the mesh displacement function $\delta\mathbf{X}=(\delta X\ ,\ \delta Y)$ on $\delta\Omega$ can be found accordingly, and this function enables us to build a new mesh on the new domain $\Omega(t+\delta t)$.

Next we seek a pair of orthogonal functions by solving Laplace equations with the following boundary conditions, as shown in Fig. 1,

$$\begin{aligned}\Psi=0\ \ on\ \ \overline{AB},\ \ \Psi=1\ \ on\ \ \overline{DC}\\ \nabla\Psi\cdot\mathbf{n}=0\ \ on\ \ \overline{AD}\ \ and\ \ \overline{BC}\\ \Phi=0\ \ on\ \ \overline{AD},\ \ \Phi=1\ \ on\ \ \overline{BC}\\ \nabla\Phi\cdot\mathbf{n}=0\ \ on\ \ \overline{AB}\ \ and\ \ \overline{DC}\end{aligned}$$

Finally we carry out an iterative process to relocate the nodal points so that their trajectory coordinates(Ψ , Φ) recover the initial values and the orthogonality of the structured grids is preserved and the distortion for unstructured grids is reduced. In Fig. 2 an unstructured triangular mesh updated with orthogonal trajectory scheme is compared with one updated without orthogonal trajectory adjustment. The distortion of the latter is significant.

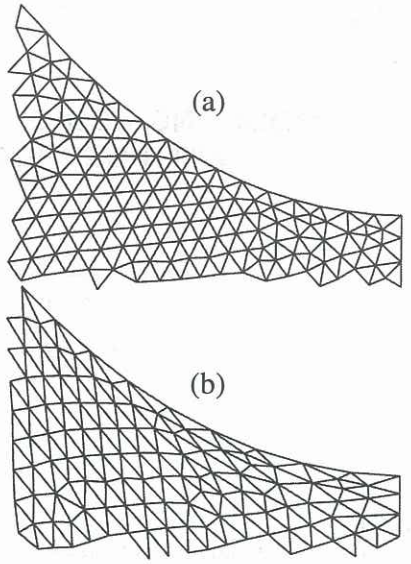

Figure 2: Triangular meshes updated with (a) and without (b) orthogonal trajectory adjustment.

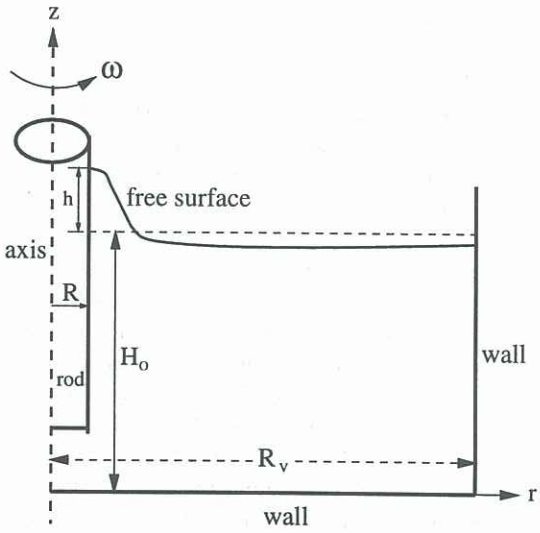

Figure 3: Flow description and boundary conditions.

RESULTS

The flow description and boundary conditions are shown in Fig. 3. A rod of radius R rotates at a constant angular speed ω about the axis of a stationary cylindrical vessel containing a viscoelastic fluid. Four dimensionless numbers are needed to characterize the rod climbing flow: the Weissenberg number Wi, Reynolds number Re, Stokes number St and the capillary number Ca, which are defined as follows:

$Wi = \lambda\omega$
$Re = \frac{\rho\omega R^2}{\eta}$
$St = \frac{\eta\omega}{\rho g R}$
$Ca = \frac{\eta\omega R}{\Gamma}$

Our numerical study mainly consists of two parts: firstly the Maxwell model is used to solve the rod climbing problem under the conditions of creeping flow ($Re = 0$), zero surface tension ($Ca = \infty$) and low angular speed, and the results are compared with perturbation theory which is valid only for small angular speed. In the second part of our numerical study the PTT model is used to simulate some real experiments of rod climbing flow by Beavers and Joseph (1975), taking into consideration all the important factors affecting the flow: surface tension, gravity, centrifugal force and second normal stress difference.

Fig. 4 compares the numerical and analytical predictions on the free surface shape, which shows the two agree very well. At low Wi the free surface shows a $1/r^4$ dependence, except near the contact point where the numerical simulation predicts a flat angle (90^o) while analytical one does not.

The difference in contact angle between numerical and perturbation analysis is an interesting one and worth some comments: experimental observations (Beavers and Joseph 1975) reveal that if there is no static wetting due to surface tension, *i.e.* no initial climbing when the fluid is stationary ($\omega = 0$), the contact angle at the rod remains flat (90^o) after the climbing and the free surface shape near the rod is convex. Since both numerical and analytical results in Fig.4 are based on zero static climbing (due to zero surface tension), the above experimental observation means our numerical prediction is more realistic than the perturbation analysis.

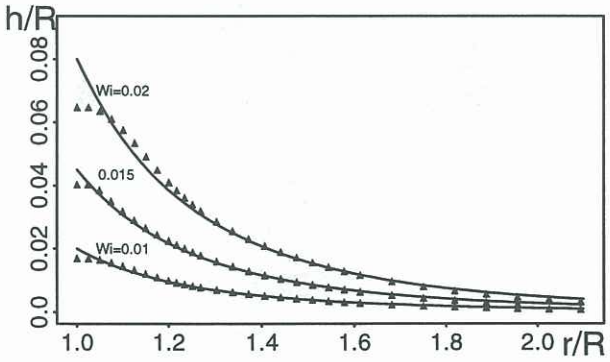

Figure 4: Predictions of the free surface shapes.
$\triangle$, this work using UCM;
—, theory (Beavers and Joseph 1975).

To realistically simulate the experiments of Beavers and Joseph (1975), the PTT model was used to cope with the non-zero second normal stress difference. In the experiments reported by Beavers and Joseph (1975), STP (a 26.6% polyisbutylene solution in petroleum oil) was used, for which the following material constants were given at temperature 25.5^oC:
$\rho = 0.89g\ cm^{-3}$
$\eta = \eta_s + \eta_m = 146\ poise$
$\Gamma = 30.9\ dyn\ cm\ s^{-2}$
$(1 - \frac{\eta_s}{\eta_m})\lambda = 0.0162\ s$
where η_s is the newtonian solvent viscosity. The radius of the rod is $R = 0.635cm$, the cylindrical vessel has a radius of $R_V = 15.25\ cm$, and the height of the fluid at rest is $7.7\ cm$.

Four material parameters in the PTT model need to be determined or estimated before starting the simulation: η_m, λ, ξ and ϵ. In the absence of direct experimental data, we have let $\epsilon = 0$ and taken the commonly used ratio $\eta_s/\eta_m = 1/9$ to determine η_m from $\eta = \eta_s + \eta_m = 146\ poise$ and the relaxation time λ from $(1 - \frac{\eta_s}{\eta_m})\lambda = 0.0162\ s$.

The second normal stress parameter ξ can be estimated from the climbing constant given by the perturbation theory:

$$\hat{\beta} = [(1 - \frac{\eta_s}{\eta_m})\lambda\eta](1 - 2\xi) \qquad (7)$$

where $\hat{\beta}$ is the climbing constant which can be measured by carrying out low angular speed experiments. For the case of STP at temperature 26^oC the experimental value of $\hat{\beta}$ was found to be $\hat{\beta} = 1.02$ (Beavers and Joseph 1975), from which and Eqn.(23) we get an estimate of $\xi = 0.284$. At 26^oC a $\hat{\beta}$ value of 0.86 gives $\xi = 0.318$.

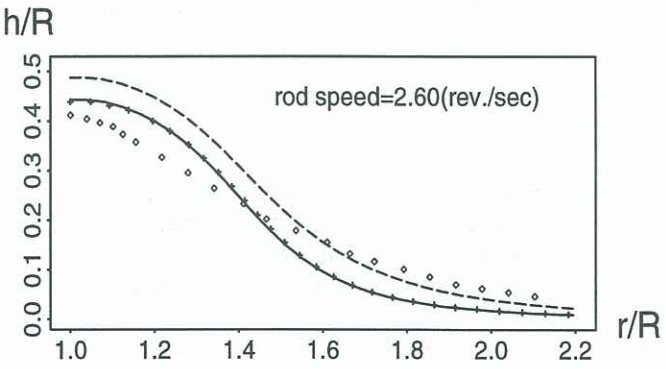

Figure 5: Predicted free surface profiles in comparison with experimental measurements with $R = 0.635$
——, triangular mesh with $\xi = 0.318$;
+, quadrilateral mesh with $\xi = 0.318$;
– – –, triangular mesh with $\xi = 0.284$;
$\diamond$, measurements by Beavers and Joseph (1975).

Figure 5 compares the predicted free surface profiles with experimental measurements with R =

0.635, showing computational results of both triangular mesh and quadrilateral mesh. The maximum absolute difference in climbing height between our prediction and the measurement is less than half a millimeter. Fig. 6 shows the final quadrilateral mesh, the final triangular mesh and the velocity vectors (in the $r - z$ plane) in the region near the contact point for the case of $\omega = 2.60$ $(rev.\ s^{-1})$ with $\xi = 0.318$. One can see the quality of the triangular mesh is still good after the relatively large deformation of the domain due to free surface movement, and the orthogonality of the quadrilateral mesh is preserved. Fig. 7 compares the numerically predicted three-dimensional free surface with the photograph presented by Beavers and Joseph (1975). The similarity of the two is satisfactory, apart from the apparent reflection in the lower half of the photo and some other optical effects in the photo.

CONCLUSION

Full finite element simulations of steady state rod-climbing flow have been performed using UCM and PTT models. The predictions are in good agreement with second-order theory and experimental data. The orthogonal trajectory scheme developed in this work is applicable to unstructured triangular mesh as well as structured quadrilateral mesh, and it provides flexibility and good quality in mesh updating for successful numerical simulation of free surface flow involving relatively large deformation in the domain. Without using the orthogonal trajectory scheme the simulation failed to converge even for very moderate climbing height.

REFERENCES

Weissenberg, K. *Nature*, 159, 310-311. 1947.

Bird, R.B., Armstrong, R.C. & Hassager, O. *Dynamics of Polymeric Liquids*, Vol. 1, John Wiley, New York, 2nd edn., 1987.

Tanner, R.I. *Engineering Rheology*, Clarendon Press, Oxford. 1985.

Barnes, H.A., Hutton, J.F. and Walters, K. *An introduction to Rheology*, Elsevier, Amsterdam, 1989.

Dean, E. Glowinski, R. Li, C.H. *Mathematics Applied to Science*, ed. Goldstein, J. Rosecrans, S. & Sod, G. (1988).

Luo, X.-L. *J. Non-Newt. Fluid Mech.*, 63 (1996) 121-140.

Beavers, G.S. and Joseph, D.D. The rotating rod viscometer, *J. Fluid Mech.*, 69 (1975) 475-511.

Fastflo Tutorial Guide (1997), CSIRO Mathematical and Information Sciences.

Mooney J.R. & de Hoog, F.R. Modelling steady state free surface flows using *Fastflo*, *Proc. 12th Australasian Fluid Mechanics Conference,* University of Sydney (1995), 407-410.

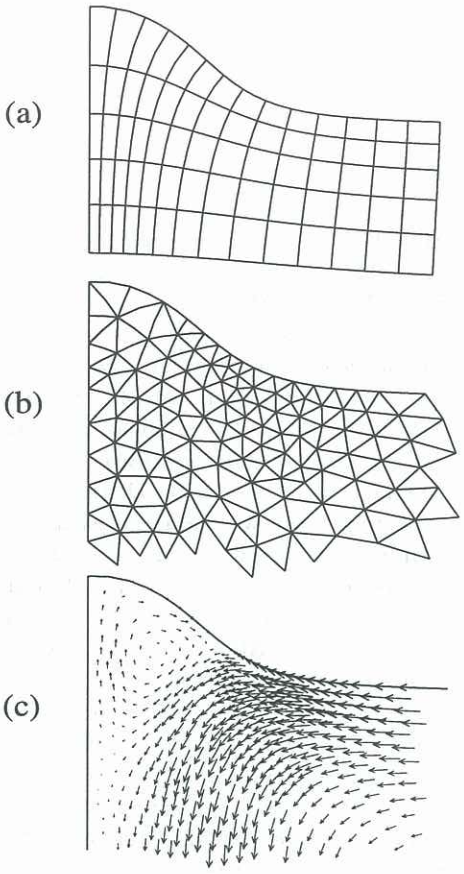

Figure 6: Final quadrilateral mesh (a), triangular mesh (b) and the velocity vectors (c) near the rod-fluid contact corner for the case of $\omega = 2.60$ $(rev.\ s^{-1})$ with $\xi = 0.318$.

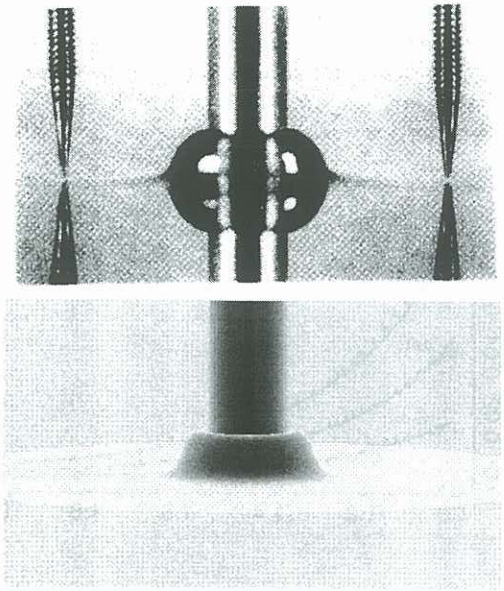

Figure 7: Three-dimensional free surface shapes for the case of $R = 0.476\ cm$, $\omega = 5$ $(rev.\ s^{-1})$. top: photo by Beavers and Joseph (1975); bottom: this work with $\xi = 0.318$.